Int. J. Electrochem. Sci., 14 **(2019)** 9311 – 9325, doi: 10.20964/2019.09.67

International Journal of ELECTROCHEMICAL SCIENCE
www.electrochemsci.org

Effect of TiO_2 Nanoparticles on the Characteristics of MAO Coatings

Ping Wang[1,2], *Xiao Wei Wei*[1,*], *Wen Jie Cao*[2], *Yi Tao Tang*[2], *Yu Wang*[2], *Ze Yu Gong*[2], *Jie Hu*[2], *Jun Pu*[2], *Xiao Tao Zu*[3]

[1] The Postdoctoral Station at Xihua University Based on Collaboration Innovation Center of Sichuan Automotive Key Parts, School of Materials Science and Engineering, Xihua University, Chengdu, 610039, China
[2] School of Materials Science and Engineering, Southwest Petroleum University, Chengdu, 610500, China
[3] School of Physics, University of Electronic Science and Technology of China, Chengdu, 611731, China
[*]E-mail: weixiaowei90@yeah.net

Received: 2 May 2019 / *Accepted:* 9 July 2019 / *Published:* 5 August 2019

Micro-arc oxidation (MAO) coatings were prepared on 2024 aluminum alloy in silicate electrolytes with the addition of TiO_2 nanoparticles with varied contents from 0 g/L to 4 g/L. The voltage-time curves, micro-hardness, thickness, surface and cross-sectional morphologies, phase composition, adhesion, corrosion resistance and the process mechanism were analyzed. The results indicated that the oxidation voltage and thickness of the coatings increased gradually with the addition of the TiO_2 nanoparticles. The coating phase composition contained TiO2. The size of the micro-pores increased, but the size of the sintered disc decreased on the surface of the MAO coatings, so the surface became more compact. Therefore, the micro-hardness and corrosion resistance of the coatings increased as the TiO2 nanoparticle concentration increased. Moreover, the adhesion of the coatings also increased because of the increase in the coating thickness. Above all, the performances of the MAO coatings with TiO2 nanoparticles were improved.

Keywords: Micro-arc oxidation; 2024 Aluminum alloy; MAO coatings; TiO_2 nanoparticles

1. INTRODUCTION

Micro-arc oxidation (MAO) is an emerging and effective surface treatment technique that is derived from anodic oxidation. MAO, known as anodic spark deposition (ASD) [1] and plasma electrolytic oxidation (PEO) [2], or micro-arc discharge oxidation (MDO) [3], is used to fabricate relatively thick in-situ ceramic coatings on light metals such as Al, Mg, Ti and their alloys to improve

their hardness and corrosion resistance [4]. Thus, as a cost-effective and environmentally friendly process, MAO has attracted great attention from researchers [5-7]. Because of high specific strength, low density and easy processability, 2024 cast aluminium alloys are generally used in engine cylinders, automobile engine pistons and craftwork 6. However, due to its relatively low hardness, poor thermal robustness, and susceptibility to surface scratch and indentation damage, 2024 aluminium alloy has been restricted from extensive use in applications 9. Because of the difference in the thermal expansion properties between MAO coatings and the matrix material, coating surfaces may exhibit micro-cracks. With the expandability of micro-cracks, the coating surface may delaminate, which ultimately results in the failure of the thermal barrier and corrosion resistance of the coating. Hence, MAO is used to enhance the properties of micro-hardness, high temperature shock robustness, adhesive strength.

In previous studies, a great number of researchers have suggested that the properties of MAO coatings are affected by the electrolytic composition, process parameters and the elements of the substrate [10]. In particular, the additives added to the electrolyte have played an important role. In recent studies, different additives, such as ZrO_2, Al_2O_3, and SiC, were incorporated to improve the micro-hardness, wear resistance and corrosion resistance of MAO coatings [11-13]. Due to its high hardness and high activity, thermal stability, good dispersion, weather resistance, and excellent electrical properties, TiO_2 nanoparticles are currently used as additives during the MAO process [6]. To date, some researchers have studied the influence of doping TiO_2 nanoparticles on MAO coatings. For example, Li [14] doped TiO_2 nanoparticles into MAO coatings on 6063 aluminum alloy, and they discovered that the reasonable TiO_2 nanoparticles concentration could enhance the micro-hardness and adhesion of the coatings. Song [15] found that the TiO_2 nanoparticles could increase the thickness and the growth rate of MAO coatings, and the corrosion resistances of coatings were also improved. Bahramian [16] added TiO_2 nanoparticles into silicate base electrolyte to obtain Al_2O_3/TiO_2 nanocomposite coatings and found found that TiO_2 nanoparticles could decrease the porosity and increase the corrosion resistance of the coatings. However, the study of doping TiO_2 nanoparticles in micro-arc oxidation coatings on 2024 aluminum alloys has not been reported.

In this study, different concentrations of TiO_2 nanoparticles were added into the silicate electrolyte to fabricate MAO coatings on 2024 aluminum alloy. Subsequently, the effects of the TiO_2 nanoparticle concentration on the coating voltage, surface and cross-sectional morphologies, phase composition, micro-hardness, thickness, adhesion, and corrosion resistance were studied, and the mechanism of forming MAO coatings is also discussed. In summary, the effect of TiO_2 nanoparticles on the characteristics of micro-arc oxidation coatings on 2024 aluminum alloy has been studied and discussed. The findings could provide an important guidance for the study of micro-arc oxidation and practical application.

2. MATERIALS AND METHODS

Samples with dimensions of 15 mm×15 mm×2 mm were cut from 2024 aluminum alloy(provided by Jinniu Xinshen Aluminum Business Department of Chengdu, China), and the chemical composition (mass fraction) is shown in Table 1. The base electrolyte was consisted of 0.2 g/L NaOH, 20 g/L

Na_2SiO_3, 2 ml/L $C_3H_8O_3$, and the concentrations of TiO_2 nanoparticles with sizes of approximately 260 nm were 0, 1, 2, 3, and 4 g/L (the abovementioned reagents were supplied by Kelong Chemical Reagent Factory and Cologne Chemicals Limited Company of Chengdu, China). To maintain homogeneity, the electrolytes containing TiO_2 nanoparticles were continuously stirred during the MAO process. A pulsed electrical power of 5 kW was used to provide a positive pulse current during the MAO process. The MAO coating was prepared in 30min with a peak current density of 10A dm^{-2}, a fixed frequency of 100 Hz and a duty cycle of 60%. The oxidation voltage-time curves were recorded. The electrolyte temperature remained lower than 30°C by a heat exchange system. After micro-arc oxidation, samples were soaked in hot water at 90°C for 20 min and then dried in warm air.

Scanning Electron Microscopy (SEM, ZEISS EVO MA15, Germany) equipped with an Energy Dispersive Spectrometer (EDS, OXFORD 20, America) were used to investigated the surface and cross-sectional morphologies of MAO coatings. The phase compositions of the coatings was observed by X-ray Diffraction (XRD, DX-2700B, China), and the diffraction data were acquired with a scattering angle of 2θ from 10° to 80° at a scanning speed of 0.1°/s. The surface micro-hardness was measured by a digital micro-hardness tester (HXD-2000TM/LCD, China) with a load of 2 N for 15 s. Ten measurements of micro-hardness were performed for every coating, and they were taken from different areas. The resulting average values are shown in Figure 6. Similarly, Digital Thickness Gauges (TT230, China) was used to tested the thickness of 10 points in different areas. Furthermore, A multifunctional surface performance tester (MFT-4000, China) was used for scratch test, and 0 ~ 30 N was automatically loaded. Each sample was tested three times in different areas. The thermal shock tests of the coatings were studied with a chamber electric furnace (SX-10-12, China) at 500°C for 10 min and then cooled down in 25°C water for 50 cycles.

A salt spray test (JK-60A, China) was used to measure the rate of corrosion, and Electrochemical Workstation (IM6, Netherlands) was applied to acquire polarization curves in 3.5% NaCl at room temperature. The polarization curve scanning rate was 1.5 mV s^{-1} with a potential range from -1.0 V to -0.4V. Especially, in the salt spray test, the specimens of MAO coatings formed with different TiO_2 concentrations were placed in 3.5% NaCl solution for 240 hours at room temperature, and the corrosion rate was calculated with the following formula:

$$V_{corr} = (m_0 - m_1)/st \quad (1)$$

where m_0 is the initial sample weight, m_1 is the weight of after corrosion, s is the sample area, and t is the corrosion time.

Table 1. The chemical composition of 2024 aluminum alloy

Cu	Mn	Mg	Cr	Zn	Si	Fe	Ti	Al
3.8-4.9	0.3-0.9	1.2-1.8	0.1	0.25	0.5	0.5	0.15	balance

3. RESULTS AND DISCUSSION

3.1 Oxidation voltage-time curve during MAO

Figure 1 shows the variety of oxidation voltages with different concentrations of TiO_2 nanoparticles. During the MAO process, the voltage rapidly increased to approximately 450 V and instantly entered into the micro-arc oxidation stage in approximately 2.5 min, and then the voltage became relatively stable. It can also be seen that with the addition of TiO_2 nanoparticles from 0 g/L to 4 g/L, the oxidation voltage increased. This can be explained by the fact that the voltage was related to the current and resistance. The resistance was the sum of the coating resistance and electrolyte resistance. When the concentration of TiO_2 nanoparticles increased, the electrolyte concentration in the solution increased, and because TiO_2 nanoparticles have negative zeta potential in alkaline media [17], more TiO_2 nanoparticles could adsorb on the surface of samples by mechanical stirring and the electric field. In addition, more electrolytes could enter into coatings through discharge channels by the electric field and mechanical stirring. With the reaction process, the resistance of the coatings increased, resulting in an increase in the total reaction resistance and ultimately an increase in the oxidation voltage. In addition, with increasing TiO_2, the rate of voltage increase was accelerated, and the breakdown voltage could be reached more quickly, so the micro-arc oxidation stage could be reached more rapidly. As a consequence, the addition of TiO_2 nanoparticles could promote the growth of MAO coatings.

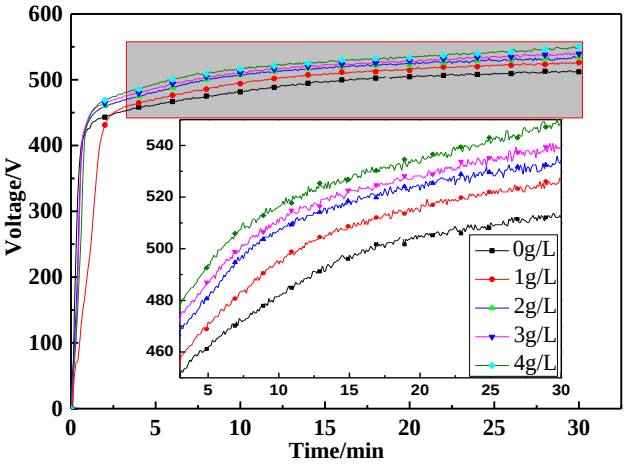

Figure 1. Voltage-time curves of the samples prepared using different concentrations of TiO_2.

3.2 The surface morphologies and EDS results of the MAO coatings

Figure 2 indicates the porous surface morphologies of the MAO coatings with different concentrations of TiO_2. There were many sintered discs and micro-pores on the surface of the coatings. The size of the micro-pores increased, but the number decreased with increasing TiO_2 concentration. In contrast, the size of the sintered disc gradually decreased with increasing TiO2 nanoparticle concentration. When the oxidation voltage reached a critical point (breakdown voltage) in the

electrolytes, the spark discharge occurred on the substrate surface. With increasing voltage, it would changed from a spark discharge to an intense micro-arc discharge on the sample surface. First, the initial discharge ignited the gas bubbles between the coating and the electrolyte and then induced the breakdown of the dielectric barrier layers. Each micro-discharge occurred in micro-pores of the oxidation film, which was attributed to an initial dielectric breakdown of a barrier layer in the bottom of the micro-pores [18]. With increasing TiO_2 nanoparticles, the voltage became higher, which supplied more energy and maintained a higher arc temperature, and the melting of the coating became more, so the size of the micro-pores increased, but the number decreased. Furthermore, because of the high energy and heterogeneous nucleation, the melt formed and deposited rapidly in the wall of the micro-pores, which led to the reduction of eruption of the melt. As a result, the sizes of the sintered discs decreased.

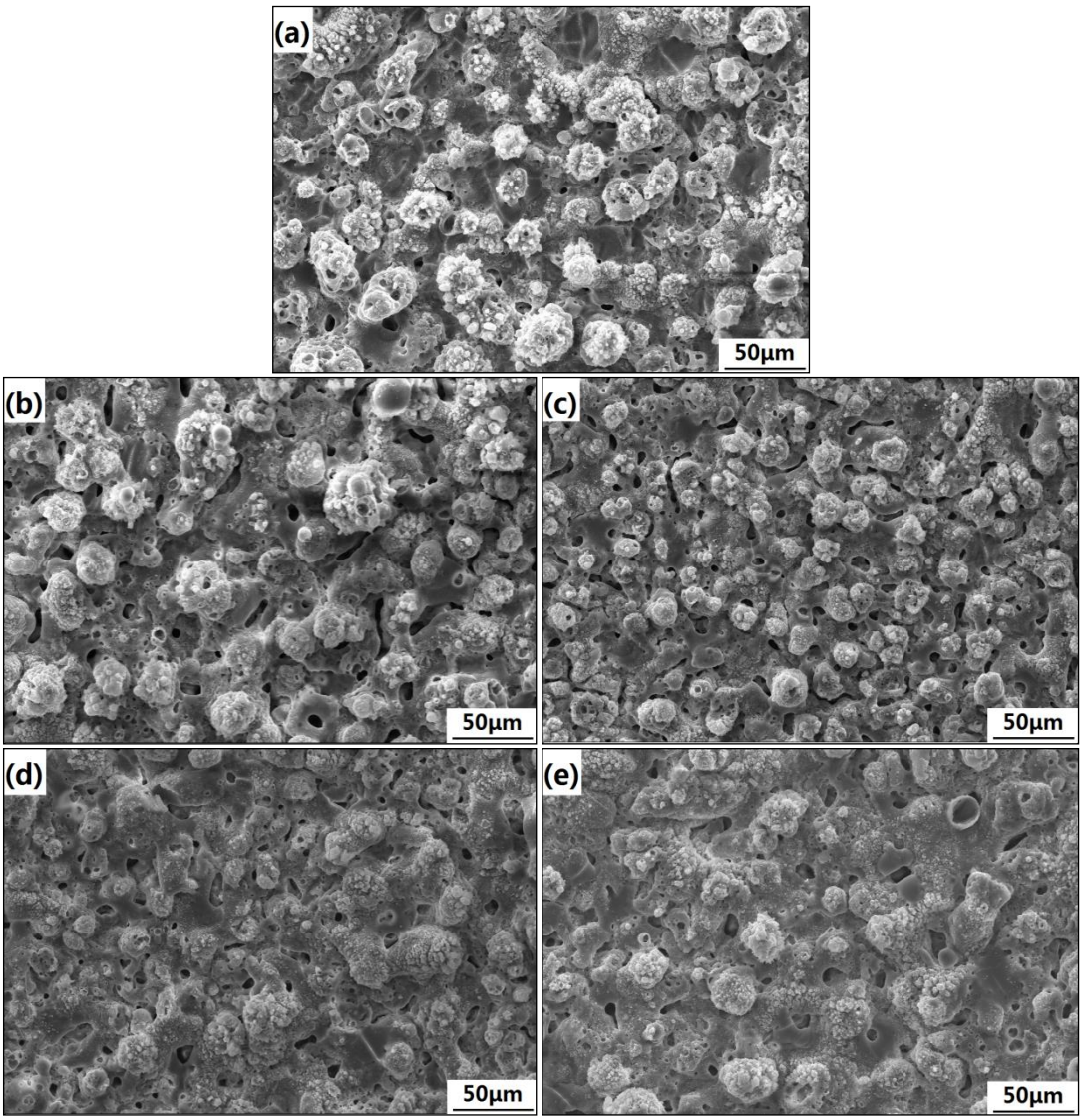

Figure 2. Surface morphologies of MAO coatings with different TiO_2 concentrations: (a) 0 g/L, (b) 1 g/L, (c) 2 g/L, (d) 3 g/L, and (e) 4 g/L.

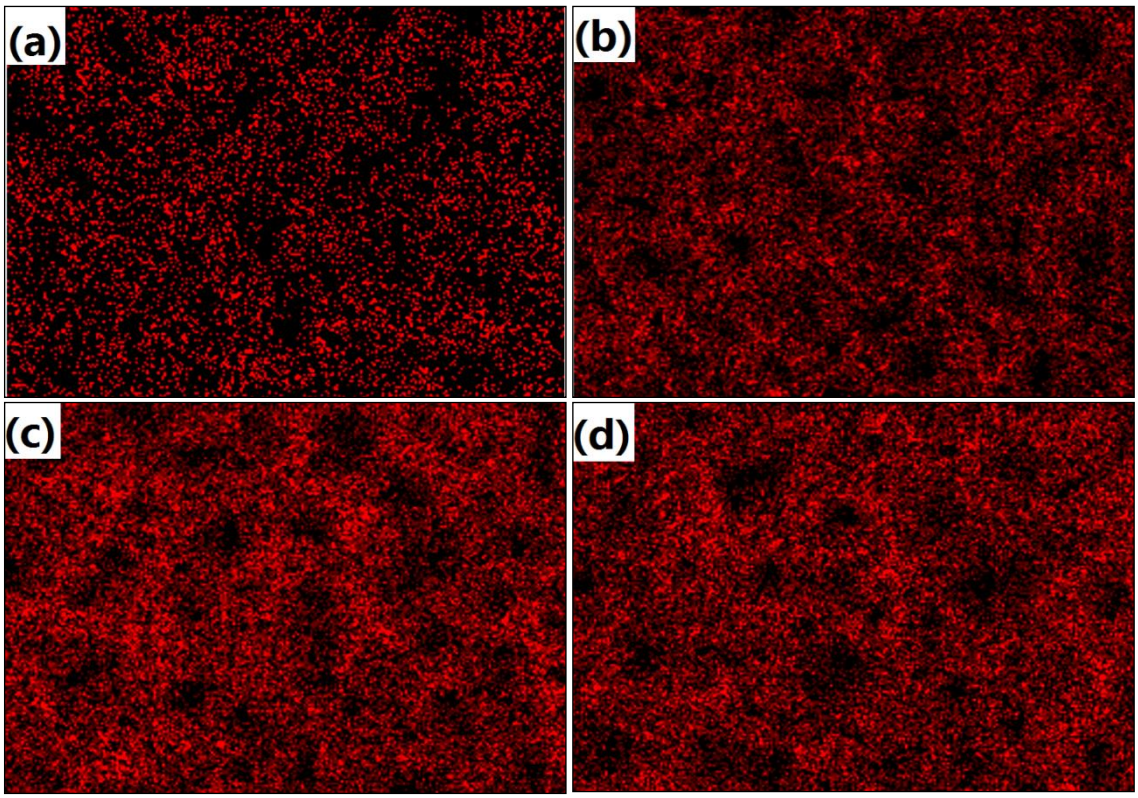

Figure 3. The distribution of Ti element on sample surface fabricated by different TiO_2 concentrations: (a) 1 g/L, (b) 2 g/L, (c) 3 g/L, and (d) 4 g/L.

Table 2 shows the element atomic fraction with different TiO_2 concentrations, and Figure 3 indicates the distribution of Ti element on the coating surface. In Figure 3, the distribution of Ti element was uniform and became denser with the addition of TiO_2 nanoparticles. From Table 2, it can be seen that the content of Si and Al decreased, O and Mg were changeless, but the content of Ti increased gradually with increasing TiO_2 concentrations. This result proved that TiO_2 nanoparticles were incorporated into the coatings successfully, which is consistent with the results shown in Figure 3.

Table 2. The element atomic fraction with different TiO_2 concentrations

Atomic (%)	Ti	O	Al	Si	Mg
0 g/L	—	49.40	14.87	35.54	0.20
1 g/L	1.14	49.78	10.64	38.24	0.19
2 g/L	4.30	48.73	14.82	31.80	0.36
3 g/L	5.00	49.67	12.35	32.62	0.36
4 g/L	5.94	48.62	11.25	33.87	0.31

3.3 The cross-section morphologies of MAO coatings

Figure 4 shows the cross-sectional morphologies of the coatings formed in electrolytes with different TiO_2 concentrations. In fact, the addition of TiO_2 affected not only the surface micro-morphologies but also the cross-sectional morphologies. From Figure 4, it can be seen that the coatings consisted of two layers, which included a loose layer (out-layer) and a dense layer (in-layer). Some micro-pores could be observed on the coating cross sections, and the adhesion of the substrates and MAO coatings was tight. Comparing the cross-sectional morphologies of Figure 4, it can be found that the thickness of the MAO coatings formed in electrolytes increased with increasing TiO_2 nanoparticle concentration. Thus, the addition of TiO_2 was beneficial for promoting the thickness of the ceramic coatings. According to Figure 1, because the oxidation voltage rose by increasing TiO_2 concentration, the higher energy in the micro-arc discharge process resulted in the increase of the arc temperature. Therefore, the coatings could be sufficiently sintered, and the materials bonded tightly with increasing TiO_2 concentration [15]. The results of EDS line scanning showed that the Ti content of the MAO coating element rose gradually, and the distribution of Ti was relatively uniform in the loose layer and dense layer of the coatings.

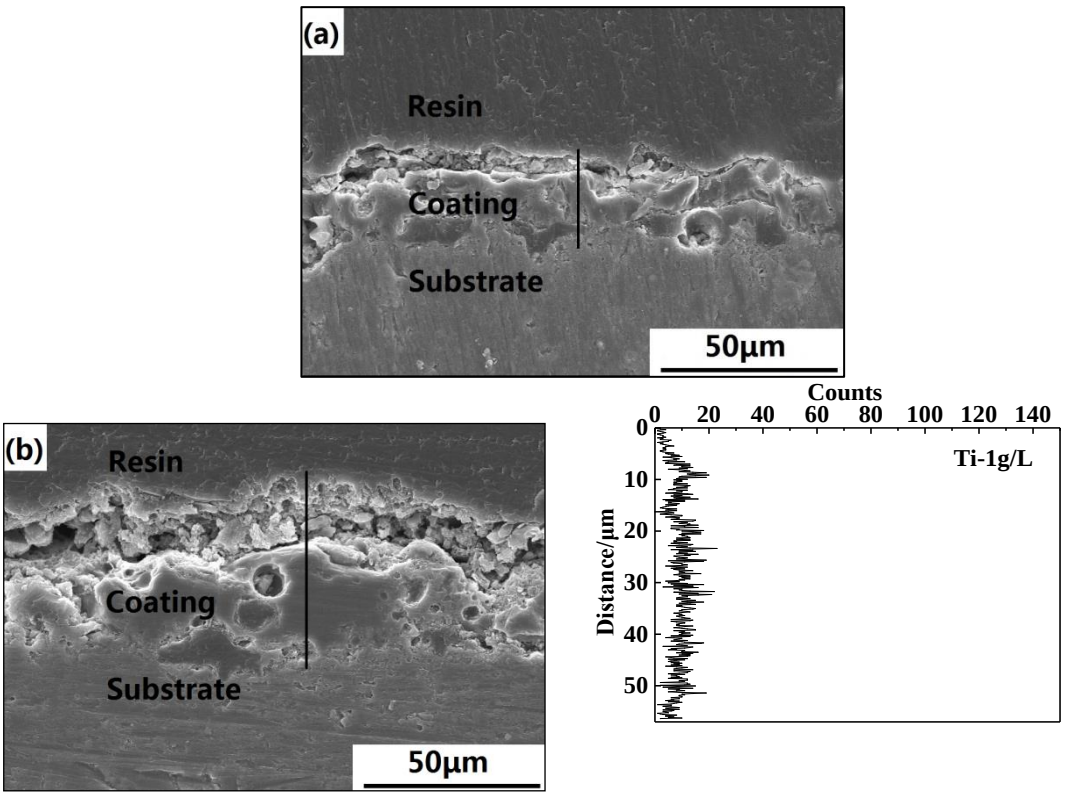

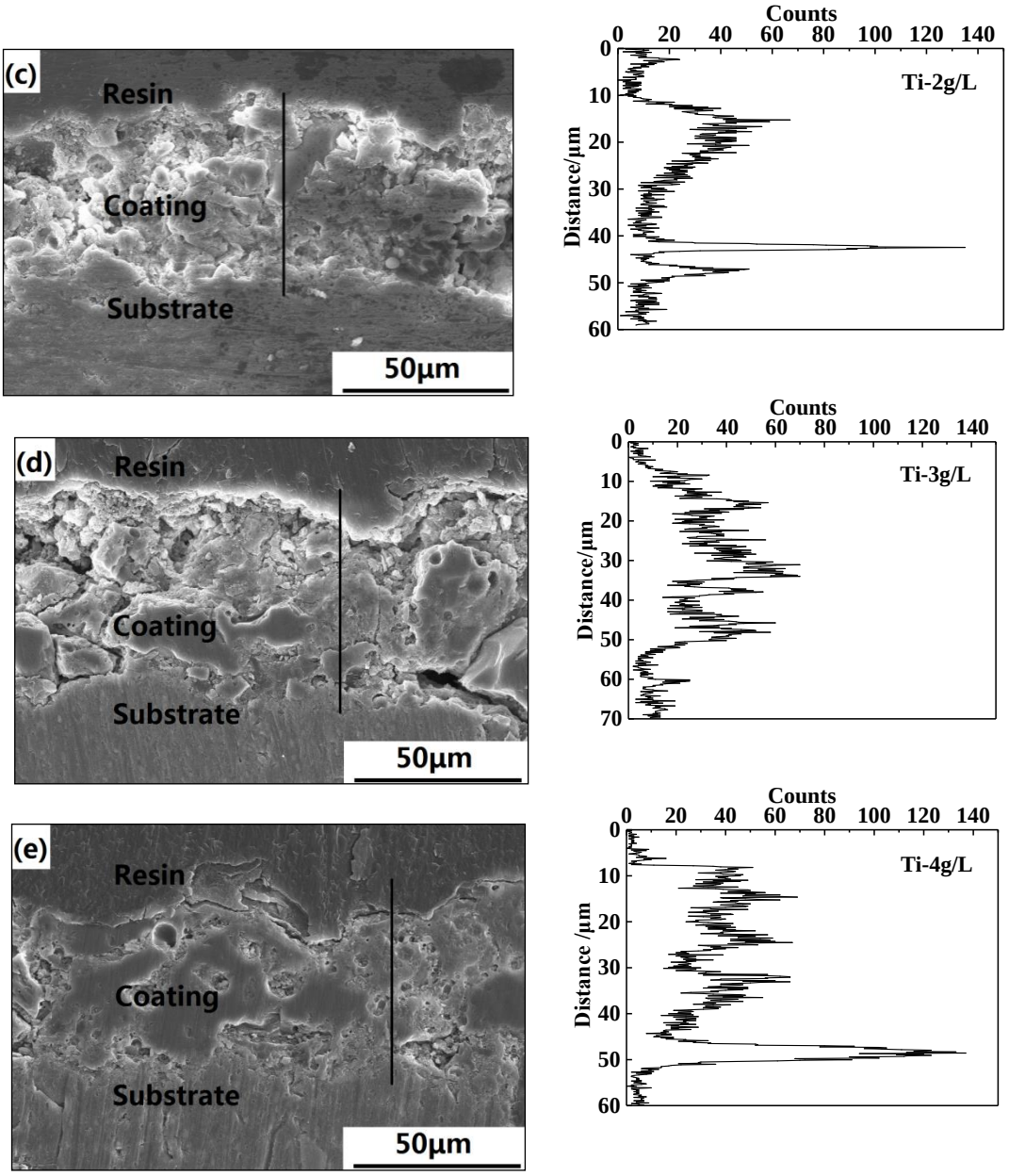

Figure 4. Cross-section morphologies and Ti distribution of MAO coatings prepared by different TiO_2 concentrations: (a) 0 g/L, (b) 1 g/L, (c) 2 g/L, (d) 3 g/L, and (e) 4 g/L.

3.4. The phase composition of the MAO coatings

The phase composition of the MAO ceramic coatings with added TiO_2 nanoparticles was investigated by XRD. As shown in Figure 5, it could be illustrated that the coatings mainly consisted of γ-Al_2O_3, SiO_2, α-Al_2O_3 and TiO_2, and the elements appearing in the phase composition were consistent with the EDS map scanning. The phase of TiO_2 appeared when TiO_2 nanoparticles were added, but the intensity of the SiO_2 and γ-Al_2O_3 changed slightly. Therefore, it could be indicated that adding TiO_2 nanoparticles did not exert an apparent influence on the phase composition of the MAO coatings. During the MAO process, some chemical reactions might have occurred as follows [14]:

$$2Al^{3+} + 6OH^- \rightarrow Al_2O_3 + 6H_2O \quad (2)$$

$$2Al^{3+} + 3{SiO_3}^{2-} \rightarrow 3SiO_2 + Al_2O_3 \quad (3)$$

$$2Al^{3+} + 3O^{2-} \rightarrow Al_2O_3 \quad (4)$$

$$\mathrm{AlOOH} \xrightarrow{300℃} \gamma - Al_2O_3 \xrightarrow{800-1200℃} \alpha - Al_2O_3 \quad (5)$$

$$TiO_2(s) \xrightarrow{micro-arc} TiO_2(melt) \xrightarrow{cooling} TiO_2(coating) \quad (6)$$

It is generally believed that the amorphous MAO alumina coating is first produced. The oxidation of aluminium initiated from 140°C, and the amorphous aluminium was oxidized into γ-Al_2O_3. Then, the surface oxidized aluminium particles started to melt, the γ-Al_2O_3 phase transformed into α-Al_2O_3 by heating in the range of 800-1200°C [5,19], and the reaction is shown by formula (5). A main idea of the transformation mechanism is that both α-Al_2O_3 and γ-Al_2O_3 phases in the MAO coatings are mainly formed through rapid cooling of the molten alumina. The critical free energy of nucleation for γ-Al_2O_3 is lower than for α-Al_2O_3 when there is a very high cooling rate [5]. When α-Al_2O_3 and γ-Al_2O_3 phases formed, at the same time, the molten TiO_2 nanoparticles entered into the discharge channels and mixed within the Al_2O_3 and then cooled rapidly.

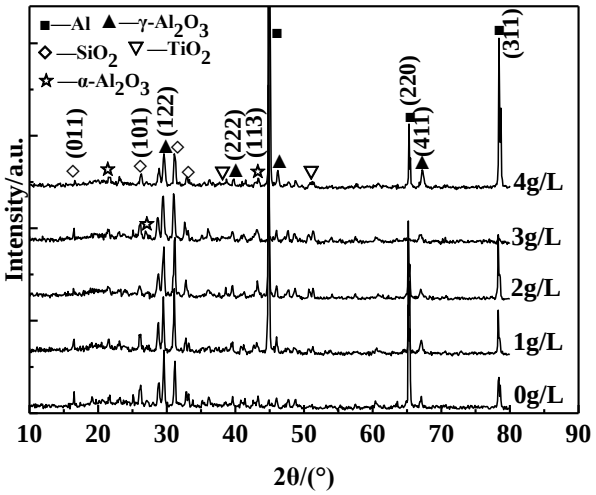

Figure 5. XRD spectrum of MAO coatings prepared by different TiO_2 concentrations.

3.5 Micro-hardness and thickness of the MAO coatings

Figure 6 presents the thickness and micro-hardness. It can be observed that the thickness and micro-hardness increased gradually with increasing TiO_2 nanoparticle concentration. First, the increase in thickness could be explained by an ejection process of molten alumina. In the process of MAO coating growth, the oxidation film formed by anodic oxidation broke down, and micro-discharges appeared as a result of the instantaneous high temperatures. Second, aluminium and elemental alloys of the substrate were melted, entered the discharge channels and were oxidized; in addition, compositions of electrolyte also entered the discharge channels. Third, due to the high temperature and voltage caused by discharge sparks, ions from the substrate and electrolyte were generated by relative chemical reactions, and then the reaction products were cooled down and deposited onto the discharge channel walls 18. Because of the increase in TiO_2, the reaction products increased, and the thickness increased. As shown in Figure 2,

with the addition of TiO_2 nanoparticles, the surface of the MAO coatings became more compact and smoother, so the micro-hardness of the ceramic coatings increased. Furthermore, the phase compositions included TiO_2, γ-Al_2O_3 and α-Al_2O_3, which possess high hardness. Therefore, the more TiO_2 nanoparticles were added, the more TiO_2 was present in the MAO ceramic coatings, and the micro-hardness was higher.

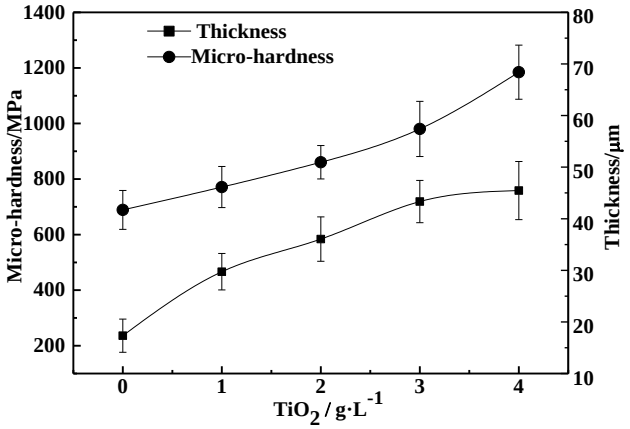

Figure 6. The micro-hardness and thickness of samples prepared by different TiO_2 concentrations.

3.6 The Crack resistance analysis

3.6.1 The adhesion strength of coatings

The results of the scratch adhesion test are shown in Figure 7 with different TiO_2 concentrations. It can be seen that with the increase of TiO_2 nanoparticles, the adhesion of the coatings increased gradually. In the test, the load at which the MAO coating scratches appeared was used as a characteristic value for the adhesion strength. Therefore, the adhesion was related to the micro-structure, thickness and micro-hardness of the coatings. As previously described, the micro-structure was increasingly compact and dense, and the thickness and micro-hardness also increased as the TiO_2 nanoparticle concentration increased. Thus, the variation trend of adhesion was consistent with the micro-hardness and thickness.

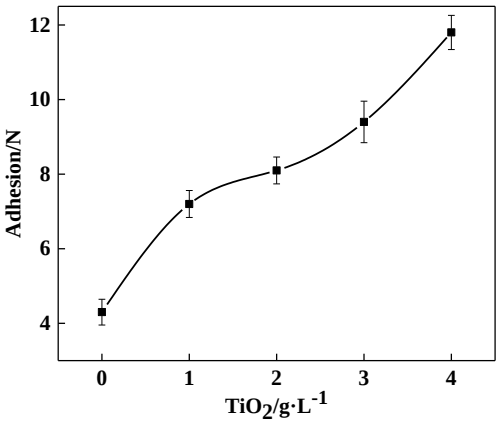

Figure 7. The average adhesion of MAO coatings prepared by different TiO_2 concentrations.

3.6.2 The thermal shock resistance of the coatings

Figures 8(a) and 8(b) show the surface morphologies of the MAO coatings with 2.0 g/L TiO_2 concentration after the thermal shock tests. There is no visible peeling in Figure 8(a), indicating the good thermal shock property of the MAO coatings. Figure 8(b) exhibits little local micro-cracking on the surface of the MAO coatings. Few micro-cracks appeared because the thermal shock stress was very high in the process of thermal shock testing, so the presence of micro-cracks could preferably release more thermal stress [12]. In addition, the rugged and porous surface of the MAO coatings caused the difference in the thermal expansion coefficients between the coatings and substrates, which had a serious effect on the combination of coatings and substrates; therefore, the initiation of micro-cracks occurred under cyclic heating conditions [20].

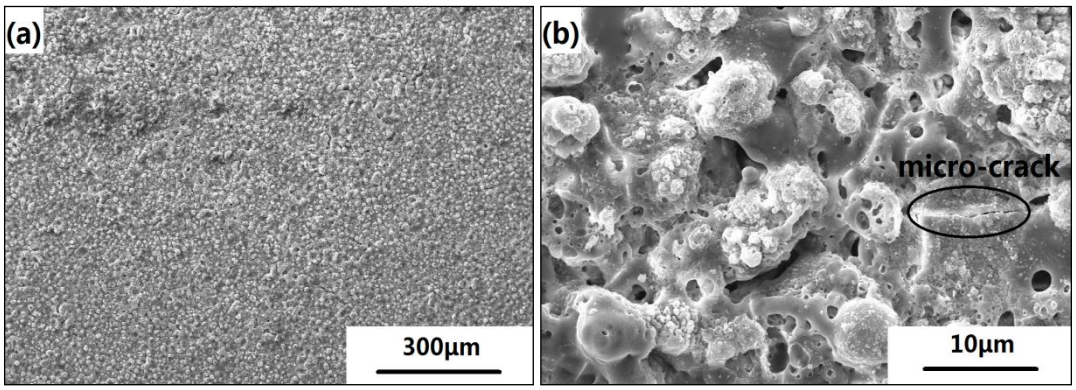

Figure 8. Surface morphologies of the coating at 2 g/L after the thermal shock tests: (a) 100 cycles, (b) 2000 cycles.

3.7 Corrosion resistance of MAO coatings

3.7.1 Salt spray test

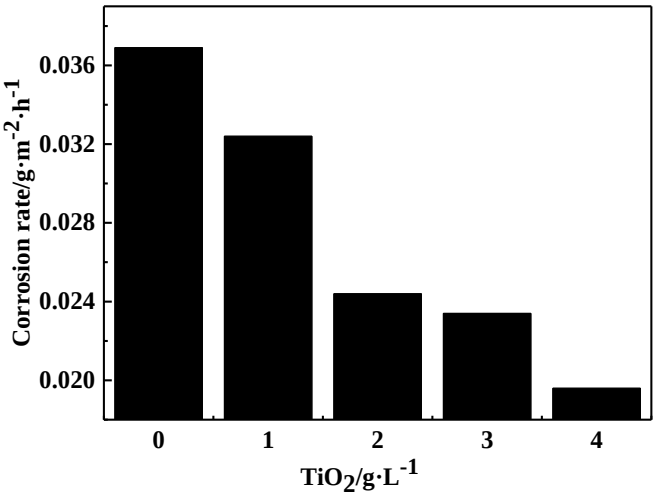

Figure 9. Corrosion rate of the MAO coatings as evaluated by the salt spray test

The rate of corrosion was tested by a salt spray test. According to formula (1), the corrosion rate can be indicated in Figure 9, and it can be seen that the corrosion rate decreased with increasing TiO_2 nanoparticle concentration. Because of the more compact and smoother surface, although the micro-pore size became larger, the corrosion rate decreased, which indicated that the corrosion resistance increased with the addition of TiO_2 nanoparticles.

3.7.2 Potentiodynamic polarization test

As shown in Figure 10, the potentiodynamic polarization curves were obtained with different TiO_2 nanoparticle concentrations, and the corrosion potential and the corrosion current density were calculated by Tafel fitting [21]. The specific calculation formulas are as follows[22]:

$$I_{corr} = \frac{\beta_\alpha \times \beta_c}{\beta_\alpha + \beta_c} \times \frac{1}{R_p} \qquad (7)$$

Then, the corrosion rate Vcorr can be acquired by the calculation formula according to Faraday law (N-equivalent weight, ρ-density):

$$V_{corr}(mil/year) = \frac{I_{coor}(A/cm^2) \times N(g) \times 393.7(mil/cm)/\rho(g/cm^3) \times 365 \times 24 \times 3600(s/year)}{96500(C/mol)} \qquad (8)$$

$$V_{corr}(mm/a) = \frac{V_{corr}(mil/year)}{39.37(mil/year)} \qquad (9)$$

The results are demonstrated in Table 3. The corrosion rate of the MAO coatings decreased, and as a result, the corrosion resistance increased, which was similar to the results of the salt spray test. According to previous analysis, the corrosion rate was influenced by the thickness of the coatings and the porosity of the micro-pores. The size of the micro-pores rose, but the surface of the MAO coatings was more compact, the coating thickness was larger, and the corrosion resistance increased with increasing TiO_2 concentration. It was obvious that the addition of TiO_2 into the electrolyte effectively improves the corrosion resistance of the MAO ceramic coatings.

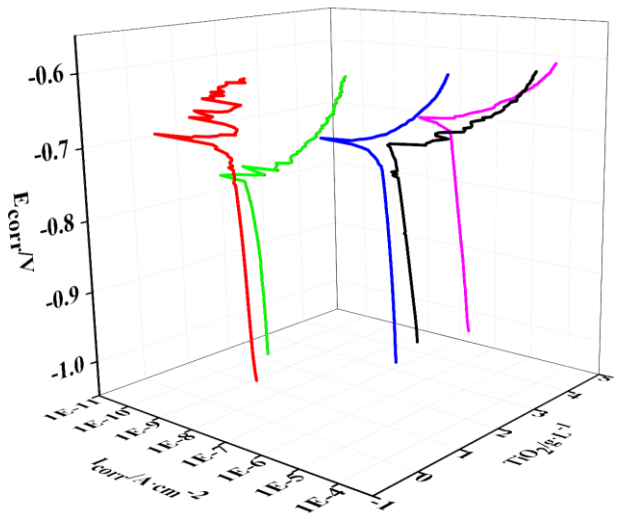

Figure 10. Polarization curves of MAO coatings at different TiO_2 concentrations.

Table 3. Corrosion electrochemical parameters of MAO coatings

TiO_2 concentration/(g/L)	E_{corr}/V	I_{corr}/(A cm^{-2})	Corrosion rate/(mm/a)
0	-0.676	1.772×10^{-8}	8.539×10^{-2}
1	-0.645	1.537×10^{-8}	7.410×10^{-2}
2	-0.662	1.344×10^{-8}	6.478×10^{-2}
3	-0.648	9.630×10^{-9}	4.641×10^{-2}
4	-0.651	5.405×10^{-9}	2.605×10^{-2}

3.8 MAO process mechanism

The growth mechanism of the MAO process is shown in Figure 11. In the circuit, the oxidation voltage increased gradually until reaching the breakdown voltage of the electrolyte, and small and free sparks began to appear at the sample surface. In fact, the initial spark discharge ignited the gas bubbles between the sample and the electrolyte and then induced the breakdown of the dielectric barrier layers. Each discharge occurred at the weak micro-areas of the oxidation coating. With the increase of voltage, the behaviour changed from spark discharges to intense micro-arc discharges on the sample surface, which led to increases in energy and temperature. Therefore, the reactions of the substrate, electrolyte and oxygen occurred, and the melting Al ejected via the discharge channels. Furthermore, TiO_2 nanoparticles with negative charge adsorbed on the surface of the sample and then entered the discharge channels by mechanical stirring and electric field. As a result, all the reaction products mixed together into the coating.

Because the oxidation voltage was relatively low at low TiO_2 concentrations compared with that at high TiO_2 concentrations, the energy and temperature were low, so the size of the micro-pores was small, and there were fewer reaction products. When the TiO_2 concentration increased, the oxidation voltage increased, and the stronger electric field induced more frequent electric arc discharge events, which enlarged the size of the discharge channels. Meanwhile, the drastic electric arc breakdown and large-sized discharge channels accelerated the movement of particles, and more TiO_2 nanoparticles and substrate were easily melted and then reacted with oxygen, which produced more reaction products; thus, the growth rate of the coating increased rapidly, and the thickness increased.

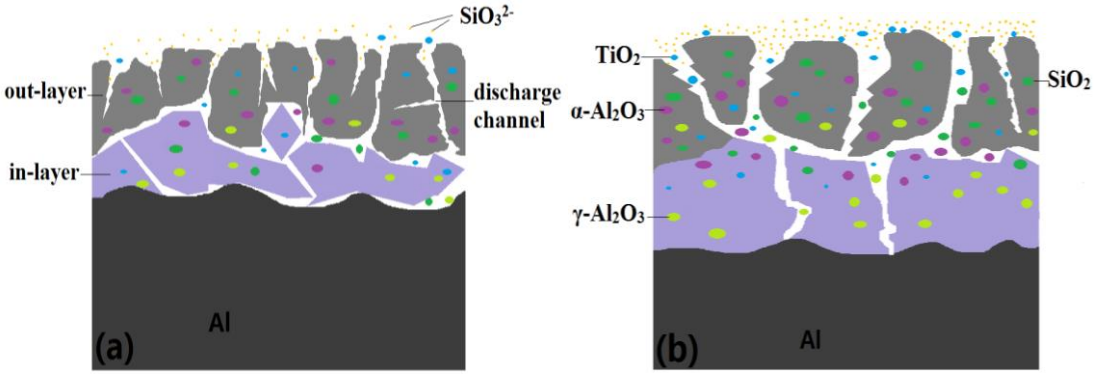

Figure 11. The mechanism of the MAO process: (a) low TiO_2 concentration, (b) high TiO_2 concentration.

4. CONCLUSIONS

MAO coatings containing TiO_2 nanoparticles were successfully fabricated on 2024 aluminium alloy in silicate electrolyte with different TiO_2 nanoparticle concentrations. With the increase in the TiO_2 nanoparticle concentration from 0 g/L to 4 g/L, because of the adsorption of TiO_2, the oxidation voltage increased, which resulted in more energy and higher temperature, and the increasing severity of the micro-arc discharge led to a decrease in the size of the sintered disc, an increase in the size of the micro-pores and more reaction products, so the surface morphologies of the coatings became denser, and the coatings thickened gradually. According to the XRD results, the coatings consisted of γ-Al_2O_3, SiO_2, α-Al_2O_3 and TiO_2, so the presence of a hard phase and a more compact microstructure caused an increase in the micro-hardness. Moreover, the adhesion rose as the micro-structure, thickness and micro-hardness increased accordingly. In addition, the corrosion resistance of MAO coatings increased because thicker and denser coatings could effectively inhibit Cl^- movement into the discharge channels. As a result, adding TiO_2 nanoparticles into the electrolyte could enhance the performance of the coatings.

ACKNOWLEDGMENT
The work was supported by the Chunhui Project of Education Ministry of China (No. Z2011074); the Support Program of Wear and Friction Surface Engineering Research Center of Sichuan Provincial Education Department and the Open Fund of Sichuan Province University Key Laboratory of oil and gas field material of Southwest Petroleum University (No. X151517KCL35).

DECLARATION OF INTEREST
The authors declare that there are no conflicts of interest regarding the publication of this paper.

References

1. K. Wang, S.S. Byeon and B.H. Koo, *Surf. Coat. Technol.* 205 (2010) 11.
2. M. Javidi and H. Fadaee, *Appl. Surf. Sci.* 286 (2013) 212.

3. G. Lv, W. Gu, H. Chen, W. Feng, M.L. Khosa, L. Li, E. Niu, G. Zhang and S.Z. Yang, *Appl. Surf. Sci.* 253 (2006) 2947.
4. S. Durdu, S.L. Aktuğ and K. Korkmaz, *Surf. Coat. Technol.* 236 (2013) 303.
5. W.B. Xue, Z.W. Deng, R.Y. Chen, T.H. Zhang and H. Ma, *J. Mater. Sci.* 36 (2001) 2615.
6. P. Wang, T. Wu, J. Li, X.H. Jia, C.L. Gong and X.Y. Guo, *Rare. Metal. Mat. Eng.* 46 (2016) 479.
7. L. Wen, Y.M. Wang, Y. Zhou, L.X. Guo and J.H. Ouyang, *Corros. Sci.* 53 (2011) 473.
8. W. Yang, B.L. Jiang, H.Y. Shi and L.Y. Xian, *J. Cent South Univ T.* 17 (2010) 223.
9. J.P. Tang, Q.F. Di, Y.B. Hu, W.C. Wang, H.J. Liang and C.X. Yang, *Acta Petrolei Sinica.* 31 (2010) 684.
10. C.S. Dunleavy, I.O. Golosnoy, J.A. Curran and T.W. Clyne, *Surf. Coat. Technol.* 203 (2009) 3410.
11. Y.S. Zhong, L.P. Shi, M.W. Li, F. He and X.D. He, *Appl. Surf. Sci.* 311 (2014) 158.
12. P. Wang, T. Wu, Y.T. Xiao, J. Pu, X.Y. Guo, J. Huang and C.L. Xiang, *J. Mater. Eng. Perform.* 25 (2016) 3972.
13. S.Y. Wang, N.C. Si, Y.P. Xia and L. Liu, *T. Nonferr. Metal. Soc.* 25 (2015) 1926.
14. H.X. Li, R.G. Song and Z.G. Ji, *T. Nonferr. Metal. Soc.* 23 (2013) 406.
15. Y.L. Song, X.Y. Sun and Y.H. Liu, *Mater. Corros*. 63 (2012) 813.
16. A. Bahramian, K. Raeissi and A. Hakimizad, *Appl. Surf. Sci*. 351 (2015) 13.
17. J.K. Jiang, G. Oberdorster and B. Pratim, *Nanoparticles and Occupational Health.* 11 (2009) 77.
18. L.J. Zhu, Z.X. Guo, Y.F. Zhang, Z.X. Li and M.L. Sui, *Electrochimi. Acta.* 208 (2016) 296.
19. D.J. Shen, J. Zou, L.L. Wu, F.F. Liu, G.L. Li, J.R. Cai, D.L. He, H.J. Ma and G.R. Jiang, *Appl. Surf. Sci.* 265 (2013) 431.
20. Y. Gu, Z.F. Wang and C.Q. Xia, *Huhan Nonferrous Metals.* 23 (2007) 33.
21. P. Wang, T. Wu, Y.T. Xiao, L. Zhang, J. Pu, W.J. Cao and X.M. Zhong, *Vacuum.* 142 (2017) 21.
22. H.P. Duan, C.W. Yan and F.H. Wang, *Electrochim. Acta*, 52(2007)3785.